

# Structural Analysis of Monoclonal Antibodies by Ultrahigh Resolution MALDI In-Source Decay FT-ICR Mass Spectrometry

Yuri E.M. van der Burgt,<sup>†</sup> David P. A. Kilgour,<sup>‡</sup> Yury O. Tsybin,<sup>§</sup> Kristina Srzentić,<sup>||</sup> Luca Fornelli,<sup>||</sup> Alain Beck,<sup>⊥</sup> Manfred Wuhrer,<sup>†</sup> and Simone Nicolardi<sup>\*,†</sup>

<sup>†</sup>Center for Proteomics and Metabolomics, Leiden University Medical Center (LUMC), PO Box 9600, 2300 RC, Leiden, The Netherlands

<sup>‡</sup>Department of Chemistry, Nottingham Trent University, Nottingham, NG11 0JN, U.K.

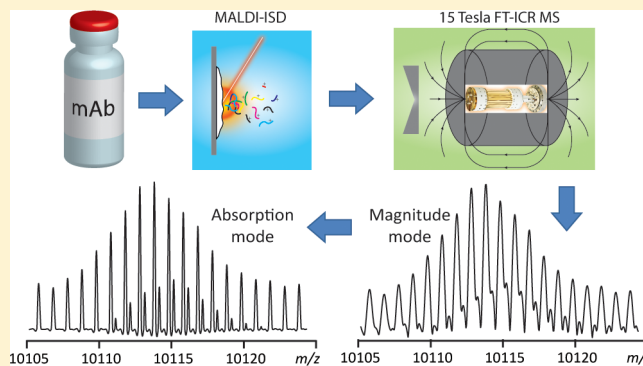
<sup>§</sup>Spectroswiss, EPFL Innovation Park, 1015 Lausanne, Switzerland

<sup>||</sup>Departments of Chemistry and Molecular Biosciences, and the Proteomics Center of Excellence, Northwestern University, 2145 N. Sheridan Road, Evanston, Illinois 60208, United States

<sup>⊥</sup>Centre d'Immunologie Pierre Fabre, 74160 St. Julien-en-Genevois, France

## Supporting Information

**ABSTRACT:** The emergence of complex protein therapeutics in general and monoclonal antibodies (mAbs) in particular have stimulated analytical chemists to develop new methods and strategies for their structural characterization. Mass spectrometry plays a key role in providing information on the primary amino acid sequence, post-translational modifications, and other structure characteristics that must be monitored during the manufacturing process and subsequent quality control assessment. In this study, we present a novel method that allows structural characterization of mAbs based on MALDI in-source decay (ISD) fragmentation, coupled with Fourier transform ion cyclotron resonance (FT-ICR) MS. The method benefits from higher resolution of absorption mode FT mass spectra, compared to magnitude mode, which enables simultaneous identification of ISD fragments from both the heavy and light chains with a higher confidence in a wide mass range up to  $m/z$  13 500. This method was applied to two standard mAbs, namely NIST mAb and trastuzumab, in preparation for method application in an interlaboratory study on mAbs structural analysis coordinated by the Consortium for Top-Down Proteomics. Extensive sequence coverage was obtained from the middle-down analysis (IdeS- and GingisKHAN-digested mAbs) that complemented the top-down analysis of intact mAbs. In addition, MALDI FT-ICR MS of IdeS-digested mAbs allowed isotopic-level profiling of proteoforms with regard to heavy chain N-glycosylation.



Structural characterization of protein therapeutics is an essential part of their development and production process.<sup>1–4</sup> Regulatory authorities require in-depth characterization, and detailed quality control, of biopharmaceuticals to demonstrate similarity of the drug substance from different batches, throughout the production process. Moreover, structural analysis provides rationale for optimizing biopharmaceuticals downstream processing and formulation studies.

The most important class of clinically approved protein therapeutics are monoclonal antibodies (mAbs) of the immunoglobulin G (IgG) class.<sup>5,6</sup> The IgG molecule has a symmetric Y-shaped structure that is composed of two identical heavy chains (Hc, approximately 50 kDa each) and two identical light chains (Lc, approximately 25 kDa each). The Hc is typically N-glycosylated at one specific asparagine in the fragment crystallizable (Fc) region.

Structural complexity in IgGs is increased by additional post-translational modifications (PTMs) such as intra- and interchain cysteine–cysteine connections (disulfide bonds), possible polypeptide truncation, and chemical modifications such as asparagine deamidation and methionine oxidation. Consequently, comprehensive structural analysis of mAbs at a proteoform level is a challenging task.<sup>7</sup> Specifically, the read-out of the primary sequence,<sup>8–10</sup> mapping of disulfide bonds,<sup>11,12</sup> and profiling of protein glycosylation<sup>13–16</sup> require various strategies that add up to a time-consuming procedure. These structural characteristics are monitored during the manufacturing process and must meet the criteria defined for the critical quality attributes of each mAb.<sup>17</sup>

**Received:** October 2, 2018

**Accepted:** December 20, 2018

**Published:** December 20, 2018

Current MS-based characterization assays of mAbs utilize primarily standard bottom-up proteomics strategies.<sup>18</sup> Sample preparation in these assays involves a reduction/alkylation step, with an inherent risk of introducing artifacts, for example when quantifying or localizing deamidation or oxidation.<sup>1</sup> Furthermore, it is well-known that a bottom-up workflow can miss detection of partial backbone cleavages or unexpected modifications.<sup>19</sup> Middle- and top-down strategies, in which the mAb is only partially digested or left intact, can largely overcome these issues.<sup>7</sup> Such approaches are mostly carried out on high-resolution electrospray ionization instruments.<sup>20,21</sup> However, matrix-assisted laser desorption/ionization (MALDI) in-source decay (ISD) MS is a powerful alternative for primary structure characterizations of both N- and C-terminal parts of proteins, including mAbs.<sup>22,23</sup> In the MALDI-ISD workflows, off-line reduction of disulfide bonds is avoided, and reduction is instead achieved by using 1,5-diaminonaphthalene (1,5-DAN) as a MALDI matrix.<sup>24,25</sup> The hydrogen-donor property of this matrix results in the reduction of the disulfide bonds during the ionization process.

In MALDI-ISD spectra, *c*-type fragment ions are usually the most intense series, while *z* + 1- (or *z* + 2), *w*-, *y*-, *b*-, and *a*-type fragments are less abundant. Most if not all fragment ions obtained from MALDI-ISD are singly charged (protonated) resulting in relatively simple mass spectra. Nonetheless, in case a mixture of proteins or polypeptide subunits is considered, such as for the analysis of an intact mAb (Hc and Lc) or its middle-down products, the complexity of MALDI-ISD spectra increases. Thus, mass measurements at ultrahigh resolution are crucial for unambiguous identification of ISD fragment ions in a wide *m/z*-range. The most frequently used instruments in MALDI-ISD MS are time-of-flight (TOF) mass analyzers that exhibit a limited resolving power.<sup>10</sup> In a previous study, we have shown that small (singly charged) proteins can be measured at isotopic resolution up to about *m/z* 17 000 using a 15T MALDI Fourier transform ion cyclotron resonance (FT-ICR) MS system and that in-depth structural information on these proteins can be obtained from ultrahigh resolution MALDI-ISD spectra (with a resolving power of 62 000 at *m/z* 16 950).<sup>26</sup> The sequence information obtained using this method was complementary to the information obtained from other fragmentation techniques. Notably, these previous measurements were performed using mass spectra represented in magnitude mode FT (mFT). The quality of FT-ICR MS data can be further improved if absorption mode FT (aFT) representation is used instead.<sup>27–30</sup>

In this study, we improved MALDI FT-ICR MS acquisition methods and complemented these with the absorption-mode FT mass spectral representation.<sup>31</sup> This was applied to analyze intact, and IdeS- and GingisKHAN-digested mAbs (NIST mAb and trastuzumab), without the need of buffer exchange, prior disulfide bond reduction, or chromatographic separation, allowing the analysis of these mAbs by MS within few minutes. The use of ultrahigh resolution MS allowed us to identify ISD fragments in a wide *m/z*-range, leading to the extensive and reliable structure characterization of mAbs.

## EXPERIMENTAL SECTION

**Chemicals.** Two different mAbs, namely trastuzumab (HzIgG1kappa, CHO) and NIST mAb standard (HzIgG1kappa, NS0), were provided by the CTDP.<sup>32</sup> Both mAbs were provided in the intact form and in a digested (but not disulfide bond reduced) form, using structure-specific enzymes IdeS or

GingisKHAN (Genovis, Lund, Sweden).<sup>33,34</sup> Briefly, intact trastuzumab and NIST mAb standard were diluted from initial concentrations of 21 and 10 mg/mL, respectively, to a final concentration of 2 mg/mL, using MQ water, and stored at  $-80$  °C in 20- $\mu$ L aliquots (in 500- $\mu$ L Lobind Eppendorf tubes) until further use.

Antibody subunits were generated in the following manner. To induce mAb cleavage below the hinge region, intact mAbs at 1 mg/mL in PBS, pH 6.8, were digested with 1000 units of Fabricator (IdeS), according to the manufacturer's instructions, at 37 °C for 30 min, under shaking (350 rpm). The reaction was quenched by adding trifluoroacetic acid to a final concentration of  $\sim 0.05\%$  and the samples were stored at  $-80$  °C until further use. To initiate mAb cleavage above the hinge region, intact mAbs at 1 mg/mL in 100 mM Tris, pH 8, were digested with 1000 units of GingisKHAN (Gingipain K), according to the manufacturer's instructions, at room temperature (RT) for 1 h. The reaction was quenched by adding trifluoroacetic acid to a final concentration of  $\sim 0.05\%$ , and the samples were stored at  $-80$  °C until further use. All samples were aliquoted and shipped on dry ice. 1,5-Diaminonaphthalene (1,5-DAN; *handle with care, check material safety data sheet*),  $\alpha$ -cyano-4-hydroxycinnamic acid (HCCA), horse myoglobin, and acetonitrile (MS grade) were purchased from Sigma-Aldrich (St. Louis, MO, USA). A stock solution of myoglobin at 2 mg/mL was prepared in water.

**MALDI-Spotting.** For ISD MS analysis, each sample (i.e., myoglobin, intact and digested mAbs) was diluted 1- to 10-fold with MQ water and spotted onto a MALDI ground steel target plate (Bruker Daltonics, Bremen, Germany) as follows. First, 1  $\mu$ L of diluted sample was put on the plate, followed by addition of 1  $\mu$ L of 1,5-DAN (saturated solution in acetonitrile/water/formic acid, 50%:49.95%:0.05%) using a 10- $\mu$ L pipet tip (Rainin tips from Mettler-Toledo, Tiel, Netherlands). Gentle mixing of the 2- $\mu$ L droplet was performed until small crystals were visible by eye; then the mixture was allowed to dry at RT. In addition, 1  $\mu$ L of diluted IdeS digest was spotted with 1  $\mu$ L of  $\alpha$ -cyano matrix (saturated solution in acetonitrile/water/formic acid, 50%:49.95%:0.05%) in a similar way. A 200  $\mu$ g/mL solution of myoglobin (1  $\mu$ L) was spotted with 1  $\mu$ L of 1,5-DAN (saturated solution in acetonitrile/water/formic acid, 50%:49.95%:0.05%) and used for external calibration of the FT-ICR MS system.

**MALDI Mass Spectrometry.** All MALDI- and MALDI-ISD FT-ICR MS experiments were performed as previously reported, with some modification of the acquisition methods.<sup>26</sup> Briefly, all MS experiments were performed on a Bruker 15 T solariX XR FT-ICR mass spectrometer equipped with a CombiSource and a ParaCell (Bruker Daltonics, Bremen, Germany). The FT-ICR MS system was controlled by ftnsControl software and equipped with a Smartbeam-II Laser System (Bruker Daltonics) that operated at a frequency of 500 Hz, and each single spectrum was generated from 200 laser shots. Higher trapping potentials (up to 9.5 V) and ParaCell DC biases (up to 9.3 V) were used to improve the mass measurement precision. Three mass spectra were obtained from a single spot, using three acquisition methods for the corresponding *m/z*-ranges: 1012–5000; 1012–7000 and 2024–30 000. A fourth acquisition method was used in the *m/z*-range 3495–30 000 for glycoform analysis. For this purpose, a second MALDI-spot was used. The measurement time ranged from 0.98 min for the acquisitions in the *m/z*-range 1012–5000 to 2.89 min for the acquisitions in the *m/z*-

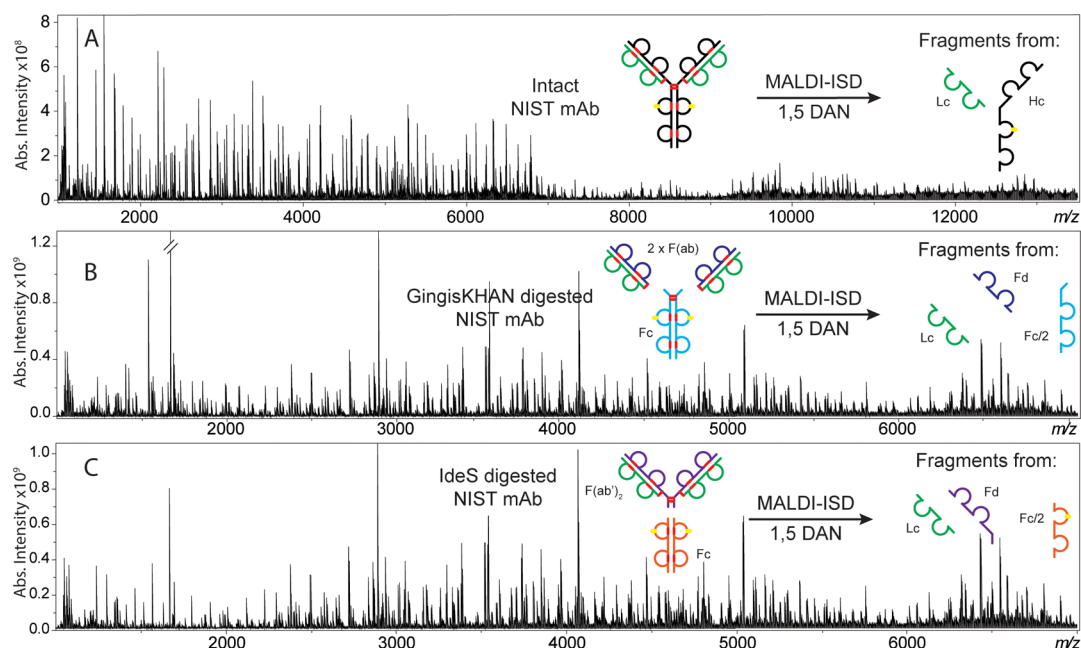


**Figure 1.** MALDI-ISD FT-ICR MS analysis of (A) intact, (B) GingisKHAN-digested, and (C) IdeS-digested NIST mAb.

range 3495–30 000. A detailed description of the FT-ICR MS parameters of the four applied acquisition methods is provided in [Supporting Information Table S1](#). The instrument was externally calibrated using ISD fragments obtained from myoglobin for the four different acquisition methods.

**Absorption Mode FT Spectra Representation.** To display an FTMS spectrum in the aFT, it is necessary to correct for systematic phase shifts across the frequency range that result from the methods used to induce coherent ion motion in the respective instruments. Various methods have been presented for solving this phase correction problem on the Orbitrap<sup>20,30</sup> and on FT-ICRs.<sup>28,29,31,35</sup> In this study, the FT-ICR MS data files were recorded to include the transient data (fid) file. The aFT mass spectra were generated directly from the transient data files using AutoVectis software suite (Spectroswiss, Lausanne, Switzerland) that incorporates an improved version of the AutoPhaser method<sup>31</sup> using a genetic algorithm<sup>35</sup> to optimize the phase correction function,<sup>36</sup> applies an asymmetric apodization function to minimize baseline deviations in the resulting absorption mode spectrum,<sup>37</sup> and generates synthetic isotopic distributions with aFT peak profiles to aid peak identification.<sup>38</sup> The data were processed by applying a full-bell, but asymmetric apodization function ( $F = 0.4$ ) to minimize baseline deviations in the resulting aFT spectrum, while allowing balance between the spectral resolution and signal-to-noise ratio across the spectrum.<sup>37</sup> After apodization, the transients were doubly zero-padded before being processed using the default AutoVectis settings. An internal calibration was applied before analysis in AutoSeequer tool. Fragment ions were assigned with an error tolerance of 10, 20, and 40 ppm for the spectra acquired with methods 1, 2, and 3, respectively (see [Table S1](#)). The tolerance for the quality value for the match between the observed and theoretical isotopic distribution was 0.65 for *c*- and *z* + 1-type fragment and 0.60 for *a*-, *b*-, *y*-, and *w*-type. An internal calibration of the spectra was also applied before spectral interpretation using mMass.<sup>39</sup> The theoretical *c*-type fragments from the Lc of each mAb were used as internal calibrants of the

spectra generated from intact mAbs while the *c*-type fragments from Fd subunit were used for the internal calibration of the spectra generated from IdeS- and GingisKHAN-digested mAbs.

**Theoretical Isotopic Distributions for Figures.** The elemental composition of ISD fragments was calculated using an in-house developed tool in Excel, and theoretical isotopic abundance distributions were generated using the online tool enviPat Web 2.2 (<http://www.envipat.eawag.ch/index.php>),<sup>40</sup> exported in the “comma-separated value” format and compiled in a text file. Plots were generated in Excel and exported in Adobe Illustrator CS6 to make the figures.

**N-Glycosylation at the Fc-Part.** N-glycosylation of the Fc-part of both NIST mAb and trastuzumab was evaluated. The IdeS-based enzymatic cleavage of NIST mAb and trastuzumab results in two identical Fc/2 parts (approximately 25 kDa each) and one F(ab)<sub>2</sub> portion (approximately 100 kDa). We analyzed IdeS digests of both NIST mAb and trastuzumab by MALDI FT-ICR MS using HCCA as MALDI matrix without the use of any additional separation.

## RESULTS AND DISCUSSION

**MALDI-ISD FT-ICR MS of Intact and Digested NIST mAb.** Intact and both IdeS- and GingisKHAN-digested mAbs were analyzed by MALDI-ISD FT-ICR MS. Ultrahigh resolution MS analysis (estimated resolving power 660 000 at *m/z* 400) was performed using three different acquisition methods to maximize both sensitivity and mass measurement precision in the *m/z* range from 1012 to 13 500 ([Figure 1](#)). Thus, obtained spectra from the analysis of intact NIST mAb are combined in [Figure 1A](#). Note that ISD fragments from both light chain (Lc) and heavy chain (Hc) are detected simultaneously. The combined spectra obtained from the analysis of IdeS- and GingisKHAN-digested NIST mAb are depicted in [Figures 1B](#) and [C](#). IdeS is an enzyme that cleaves the Hc of the NIST mAb below the hinge region, between G239 and G240, whereas GingisKHAN cleaves above the hinge region, between K225 and T226.<sup>33,34</sup> The application of

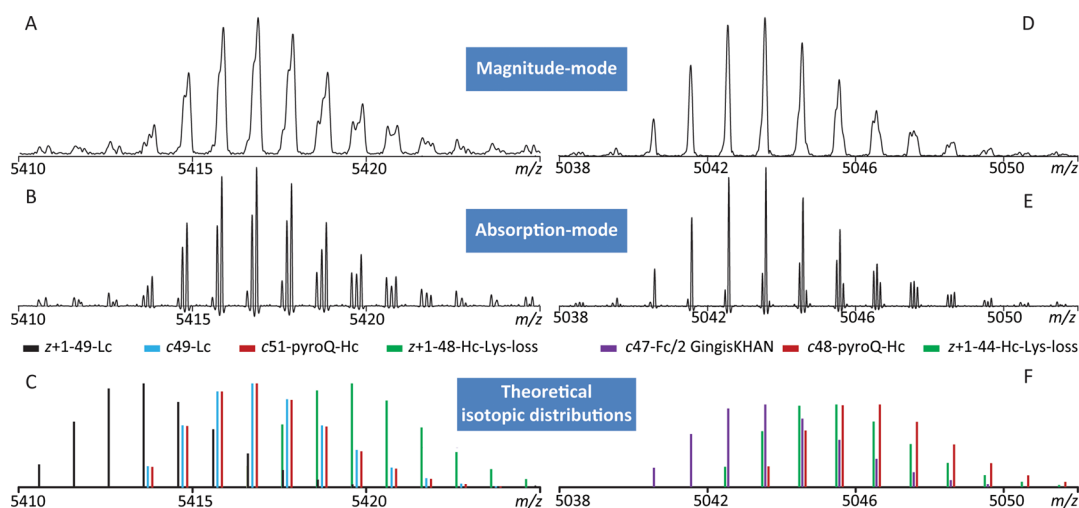


**Figure 2.** Expanded views of MALDI-ISD FT-ICR mass spectra of NIST mAb showing the increased resolving power obtained after phase correction of mFT mass spectra.

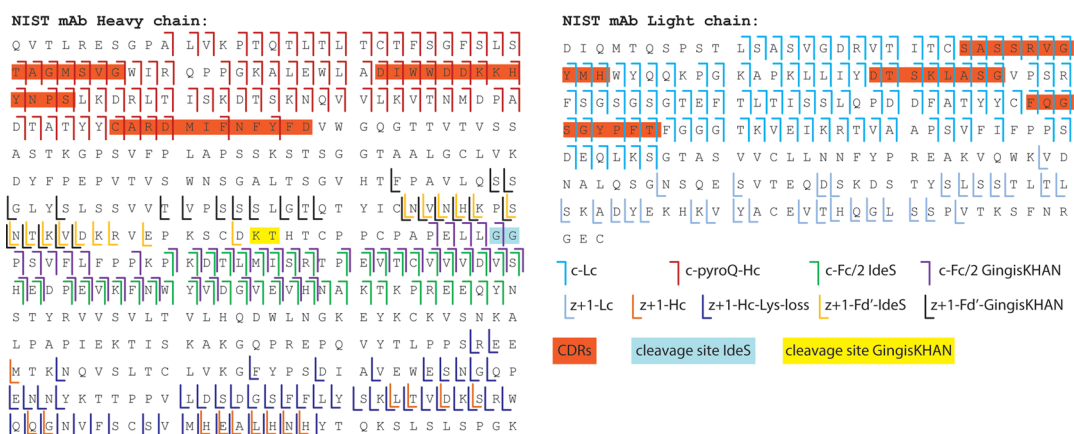


**Figure 3.** Sequence coverage obtained from the top-down and middle-down analysis of NIST mAb. Total sequence coverage was 50% and 65% for Hc and Lc, respectively. Next to glycosylation, two additional proteoforms of the Hc were identified, namely a pyro-glutamine modification at the N-terminus and a lysine loss at the C-terminus.

1,5 DAN reduces the disulfide bonds during the MALDI process. Thus, ISD fragment ions were simultaneously generated from intact Lc, Fd, and Fc/2 digestion products. The increased complexity of the IdeS/GingisKHAN-digested mAb samples hampers unambiguous fragment ion assignments especially at higher  $m/z$ -values (both in magnitude and absorption mode). Consequently, fragment ions from digested NIST mAb were assigned up to  $m/z$  7000, whereas fragment ions from intact NIST mAb were assigned up to  $m/z$  13 500.

**Magnitude-Mode FT versus Absorption-Mode FT Mass Spectra.** Resolving power is a key parameter in MS-based analysis of complex samples. Overlapping peaks can result in ambiguous identifications when mass resolution is not sufficient. FT-ICR MS provides the highest resolving power within the different classes of mass spectrometers and allows for the analysis of extremely complex samples such as petroleum,<sup>41</sup> mixtures of biomolecules,<sup>42</sup> and nanomaterials.<sup>43</sup>

However, ultrahigh mass resolution (UHMR) requires longer measurement time (seconds) with inherently reduced sensitivity. Therefore, the measurement time was balanced with ion intensities resulting in a maximum resolving power of 660 000 (magnitude mode FT, estimated at  $m/z$  400, see Table S1) for MALDI-ISD FT-ICR MS measurements. To

further improve resolving power the acquired ICR transients were processed to obtain aFT mass spectra. To this end, we used AutoVectis software to perform a phase correction of ICR time-domain data with reduced baseline deviations. The results of such a correction, in terms of improved resolving power and increased identification confidence, are exemplified in Figure 2. Here, magnitude-mode visualization did not allow the resolution of the isotopic distributions of the fragments  $c_{49}$  of the Lc and of the fragment  $c_{51}$  and  $z + 1_{48}$  of the Hc with pyro-glutamate at the N-terminus and a lysine loss at the C-terminus (Figure 2A). The postacquisition phase correction increased the resolving power and thus resolved the three isotopic distributions (Figure 2B). Note that the observed and theoretical isotopic distribution of the  $z + 1_{49}$  of the Lc did not match, thus this fragment was not identified and not included in the sequence coverage (Figure 3). Similarly, the isotopic distribution of the fragment  $c_{47}$  of the Fc/2 fragment and Lc and the fragments  $c_{48}$  and  $z + 1_{44}$  of the Hc with pyroglutamate at the N-terminus and a lysine loss at the C-terminus that were not resolved in the mFT mass spectrum (Figure 2D) could be distinguished after phase correction in the aFT mass spectrum (Figure 2E).

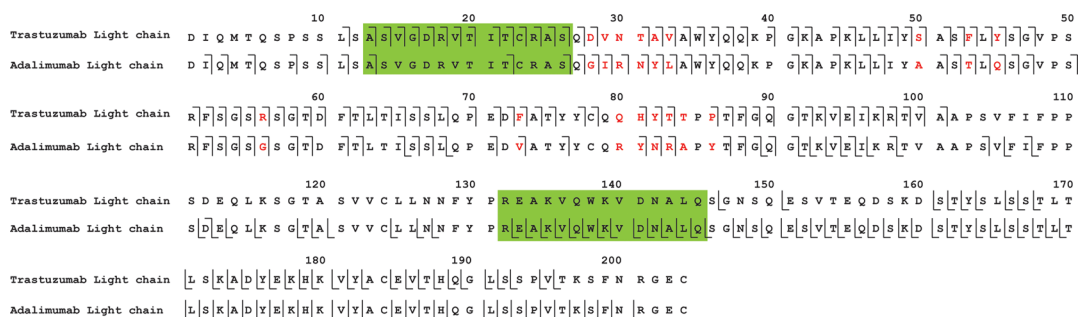


**Figure 4.** Sequence coverage of light chain obtained from the top-down MALDI-ISD FT-ICR MS analysis of trastuzumab compared to previously reported middle-down analysis by LC-MS/MS with electron-transfer dissociation of adalimumab. The two methods resulted in complementary sequence information as exemplified in the areas highlighted in green. The differences in amino acid sequence between trastuzumab and adalimumab are reported in red.

**Identification of ISD Fragment Ions.** The identification of ISD fragment ions was performed using AutoVectis. In addition, ISD spectra were visually inspected and matched to theoretical isotopic distributions of fragment ions (Figure S1). As described in the Experimental Section, we used three different acquisition methods to obtain optimal sensitivity in different  $m/z$  ranges. The sequence coverages for intact and IdeS-digested NIST mAb were obtained using these methods and AutoVectis (Figures S2 and S3). As an example, the mass measurement errors of all  $c$ - and  $z + 1$ -type fragment ions identified in the MALDI-ISD FT-ICR MS spectrum of IdeS-digested NIST in the  $m/z$ -range 1000–7000 are reported in Figure S4.

Most of the fragment ions were identified in both mFT and aFT spectra and only a minor part were identified exclusively in aFT spectra (data not shown). Phase correction led to additional identifications only when isotopic distributions were not resolved in mFT, for example, in the cases depicted in Figure 2.

MALDI-ISD analysis of the same mAb samples has also been performed using TOF MS. It is noted, however, that TOF MS instruments exhibit a lower resolving power, with corresponding limitations, even when Lc and Hc are analyzed separately. Overlapping isotopic distributions can result from fragment ions of different forms of the same chain. For example, the heavy chain  $c_{52}$  fragment ion with N-terminal pyroglutamate and the  $z + 1_{49}$  fragment ion from the Hc with a C-terminal lysine-loss have monoisotopic peaks located at  $m/z$  5528.871 and 5529.664, respectively (Figure S5). These fragment ions are baseline-resolved by FT-ICR MS but not by TOF MS.<sup>10</sup> In addition to  $c$ -type ions, the most intense fragment in the spectra, and  $z + 1$ -type ions, other fragment types were detected and identified. Examples of  $y$ -,  $b$ -,  $a$ -, and  $w$ -type fragments are depicted in Figure S6. In addition, we identified these fragment types in the MALDI-ISD FT-ICR MS spectrum generated from the analysis of IdeS-digested NIST mAb in the  $m/z$ -range 1000–7000 (Figure S7). Considering the total number of fragment ions identified in this spectrum (see Figures S3 and S7), the percentage of  $c$ -,  $z + 1$ -,  $w$ -,  $a$ -,  $y$ -, and  $b$ -type were 42%, 22%, 12%, 11%, 11%, and 2%, respectively.

The identification of different fragment ion types improves the confidence in the structural characterization of mAbs. In fact, less frequent fragment ions can be used either to corroborate the identifications based on  $c$ - and  $z + 1$ -type ions or to identify amino acids adjacent to prolines. A drawback of additional fragment types is that the signal intensity is

distributed over many more fragment ions with a consequent reduction of the signal-to-noise (S/N). In addition, the presence of many fragment types complicates the ISD spectra, making their interpretation more difficult. At last, with a higher number of fragment ions the false discovery rate (FDR) must be evaluated when identifications are not manually confirmed.

**Sequence Coverage of NIST mAb.** In this study, we have developed a fast characterization method based on ultrahigh resolution MALDI-ISD FT-ICR MS for the analysis of mAbs. This method allowed the direct analysis of mAbs without the need of a buffer exchange or a chromatographic separation of Lc and Hc or Fd' and Fc/2 digestion products. Using this method, two modifications on Hc of the NIST mAb were identified beyond glycosylation profiling, namely a pyroglutamate at the N-terminus and a lysine-loss at the C-terminus. The frequency of these two modifications was estimated at 100% and 50%, respectively. The analysis of intact NIST mAb resulted in a sequence coverage of 31% and 65% for Hc and Lc, respectively (Figure 3). The analysis of both IdeS and GingisKHAN digests increased the sequence coverage for the Hc up to 50%. The total sequence coverage for the complementarity-determining regions (CDRs) was 72% and 96% for Hc and Lc, respectively.

**Sequence Coverage of Trastuzumab mAb.** MALDI-ISD FT-ICR MS was also used to analyze trastuzumab. As for the NIST mAb, the high resolving power allowed the reliable identification of different types of ISD fragments in a wide mass range. The sequence coverage obtained from the identification of  $c$ - and  $z + 1$ -type fragment ions is reported in Figure S8. The analysis of the intact trastuzumab led to sequence coverages of 29% and 56% for Hc and Lc, respectively, while the analysis of both IdeS and GingisKHAN digests allowed to increase the sequence coverage for Hc to 49%. The total sequence coverage for the CDRs was 93% and 80% for Hc and Lc, respectively. In a recent report, trastuzumab was analyzed by ETD and HCD fragmentation.<sup>44</sup> Our MALDI FT-ICR MS analysis of trastuzumab provided sequence information that was complementary to the information obtained. Also compared to similar IgG mAbs using other fragmentation techniques MALDI-ISD FT-ICR MS data is complementary.<sup>9,45–47</sup> This is exemplified for adalimumab (middle-down LC-MS/MS using electron-transfer dissociation) in Figure 4.<sup>9</sup>

In general, the sequence coverage obtained using mFT or aFT data were similar. In fact, the number of fragment ions identified in mFT spectra ranged from 95% to 100% the number of fragment ions in the corresponding aFT spectra.

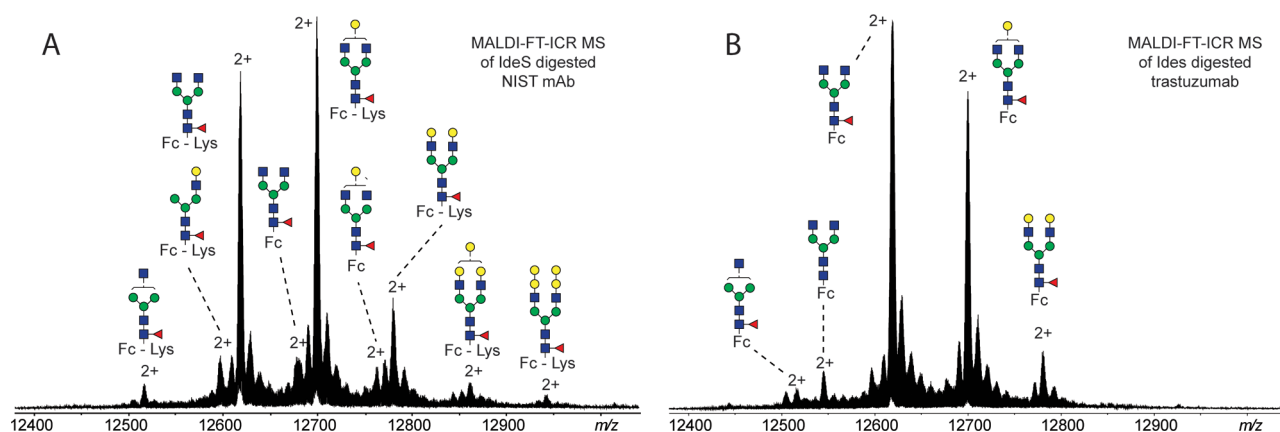


**Figure 5.** Microheterogeneity of Fc-glycosylation. MALDI FT-ICR MS spectra of IdeS-digested mAbs: (A) NIST mAb and (B) trastuzumab. For NIST mAb at least seven different N-glycans are observed at the Fc-part of Hc (detected as  $[M + 2H]^{2+}$  ions).

This is rationalized by the fact that the resolving power in mFT was already sufficient to identify most of the fragment ions. Only a minor part of all identified fragment ions were identified solely in aFT spectra. However, the identification in aFT is more reliable since a higher resolution allows detection of possible overlapping species.

**Glycosylation Analysis.** The MALDI FT-ICR MS strategies we report here also provide insight into N-glycosylation of the Fc-part of both NIST mAb and trastuzumab. Previously, in-depth glycosylation analysis resulted in the identification of tens of different glycan structures on the Hc of the IgG1 mAb.<sup>48</sup> Most of these proteoforms (glycoforms) were detected as minor components, whereas a few diantennary glycans represented more than 90% of the total glycosylation.<sup>49</sup> The analysis of these major proteoforms has been reported using lower resolution MS in combination with up-front separation.<sup>49,50</sup> The high-resolution mFT spectra of IdeS-digested NIST mAb and trastuzumab are depicted in Figure 5. The most abundant glycoforms of Fc-parts of both NIST mAb and trastuzumab are observed as doubly charged ions and, for the first time, identified at isotopic resolution. The relative abundance of these glycoforms is in good agreement with previously reported characterization studies of these mAbs.<sup>49,50</sup>

## CONCLUSIONS

We have developed a novel strategy based on ultrahigh resolution MALDI-MS FT-ICR MS to characterize mAbs. This strategy was applied to primary structure and proteoform analysis of two IgG1 mAbs, namely NIST mAb standard and trastuzumab. Complex top- and middle-down MALDI-MS FT-ICR mass spectra were generated from both intact mAbs and their large, 25–50 kDa, subunits, produced via IdeS- and GingisKHAN-based digestion. It was shown that MALDI-MS fragment ions were complementary to those observed in electron-transfer dissociation experiments, and thus translated in additional sequence coverage of the mAbs. It is noted that the combination of top-down and middle-down experiments increased total sequence coverage, however IdeS- and GingisKHAN-based digestions are not needed to map the antibody CDRs.

Postprocessing of transients (using AutoVectis) was used to generate absorption-mode FT mass spectra with improved resolving power resulting in unambiguous assignments of further resolved fragment ions. It is noted that although

sequence coverage hardly increased, the superior quality of aFT spectra led to a more confident characterization of both N- and C-terminal parts of NIST mAb and trastuzumab compared to mFT mass spectra of the same samples.

Finally, direct analysis of IdeS digests by MALDI FT-ICR MS provided a snapshot of the most abundant Fc-glycans that agreed with previously reported in-depth microheterogeneity analysis of mAb Fc-glycosylation. We envision integration of this strategy into a multimethod approach designed for the in-depth structural characterization of complex proteins such as mAbs.

## ASSOCIATED CONTENT

### Supporting Information

The Supporting Information is available free of charge on the ACS Publications website at DOI: 10.1021/acs.analchem.8b04515.

Table S1 and Figures S1–S8 as noted in the text (DOCX)

## AUTHOR INFORMATION

### Corresponding Author

\*E-mail: s.nicolardi@lumc.nl.

### ORCID

Yury O. Tsybin: 0000-0001-7533-0774

Manfred Wührer: 0000-0002-0814-4995

Simone Nicolardi: 0000-0001-8393-1625

### Notes

The authors declare the following competing financial interest(s): Dr. Tsybin and Dr. Kilgour co-develop AutoVectis software, which is available as either open-source, freeware or commercially so a financial conflict of interest is declared.

## ACKNOWLEDGMENTS

This work was performed in anticipation of an interlaboratory study of mAbs (Pilot Project) initiated and coordinated by the Consortium for Top-Down Proteomics (CTDP); <http://www.topdownproteomics.org/initiatives/monoclonal-antibody-project/>.<sup>32</sup> We greatly appreciate the support of the Pilot Project by the CTDP and its supporting organizations, Thermo Fisher Scientific Inc., Bruker Corp., and Genovis AB.

## REFERENCES

- (1) Beck, A.; Terral, G.; Debaene, F.; Wagner-Rousset, E.; Marcoux, J.; Janin-Bussat, M.-C.; Colas, O.; Dorsselaer, A. V.; Cianferani, S. *Expert Rev. Proteomics* **2016**, *13*, 157–183.
- (2) Zhang, H.; Cui, W.; Gross, M. L. *FEBS Lett.* **2014**, *588*, 308–317.
- (3) Srebalus Barnes, C. A.; Lim, A. *Mass Spectrom. Rev.* **2007**, *26*, 370–388.
- (4) Bradbury, A.; Pluckthun, A. *Nature* **2015**, *518*, 27–29.
- (5) Scott, A. M.; Wolchok, J. D.; Old, L. J. *Nat. Rev. Cancer* **2012**, *12*, 278–287.
- (6) Weiner, G. J. *Nat. Rev. Cancer* **2015**, *15*, 361–370.
- (7) He, L.; Anderson, L. C.; Barnidge, D. R.; Murray, D. L.; Hendrickson, C. L.; Marshall, A. G. *J. Am. Soc. Mass Spectrom.* **2017**, *28*, 827–838.
- (8) Ayoub, D.; Jabs, W.; Resemann, A.; Evers, W.; Evans, C.; Main, L.; Baessmann, C.; Wagner-Rousset, E.; Suckau, D.; Beck, A. *mAbs* **2013**, *5*, 699–710.
- (9) Fornelli, L.; Ayoub, D.; Aizikov, K.; Beck, A.; Tsybin, Y. O. *Anal. Chem.* **2014**, *86*, 3005–3012.
- (10) Resemann, A.; Jabs, W.; Wiechmann, A.; Wagner, E.; Colas, O.; Evers, W.; Belau, E.; Vorweg, L.; Evans, C.; Beck, A.; Suckau, D. *mAbs* **2016**, *8*, 318–330.
- (11) Wang, Y.; Lu, Q.; Wu, S. L.; Karger, B. L.; Hancock, W. S. *Anal. Chem.* **2011**, *83*, 3133–3140.
- (12) Wu, S. L.; Jiang, H.; Lu, Q.; Dai, S.; Hancock, W. S.; Karger, B. L. *Anal. Chem.* **2009**, *81*, 112–122.
- (13) Reusch, D.; Habberger, M.; Falck, D.; Peter, B.; Maier, B.; Gassner, J.; Hook, M.; Wagner, K.; Bonnington, L.; Bulau, P.; Wuhrer, M. *mAbs* **2015**, *7*, 732–742.
- (14) Tran, B. Q.; Barton, C.; Feng, J.; Sandjong, A.; Yoon, S. H.; Awasthi, S.; Liang, T.; Khan, M. M.; Kilgour, D. P. A.; Goodlett, D. R.; Goo, Y. A. *J. Proteomics* **2016**, *134*, 93–101.
- (15) Yang, Y.; Wang, G.; Song, T.; Lebrilla, C. B.; Heck, A. J. R. *mAbs* **2017**, *9*, 638–645.
- (16) Rosati, S.; van den Bremer, E. T.; Schuurman, J.; Parren, P. W.; Kamerling, J. P.; Heck, A. J. *mAbs* **2013**, *5*, 917–924.
- (17) Reusch, D.; Tejada, M. L. *Glycobiology* **2015**, *25*, 1325–1334.
- (18) Beck, A.; Wagner-Rousset, E.; Ayoub, D.; Van Dorsselaer, A.; Sanglier-Cianferani, S. *Anal. Chem.* **2013**, *85*, 715–736.
- (19) Bogdanov, B.; Smith, R. D. *Mass Spectrom. Rev.* **2005**, *24*, 168–200.
- (20) Srzentic, K.; Nagornov, K. O.; Fornelli, L.; Lobas, A. A.; Ayoub, D.; Kozhinov, A.; Gasilova, N.; Menin, L.; Beck, A.; Gorshkov, M.; Aizikov, K.; Tsybin, Y. O. *Anal. Chem.* **2018**, *90*, 12527–12535.
- (21) Mao, Y.; Valeja, S. G.; Rouse, J. C.; Hendrickson, C. L.; Marshall, A. G. *Anal. Chem.* **2013**, *85*, 4239–4246.
- (22) Ait-Belkacem, R.; Berenguer, C.; Villard, C.; Ouafik, L. H.; Figarella-Branger, D.; Beck, A.; Chinot, O.; Lafitte, D. *mAbs* **2014**, *6*, 1385–1393.
- (23) Bakalarski, C. E.; Gan, Y.; Wertz, I.; Lill, J. R.; Sandoval, W. *Nat. Biotechnol.* **2016**, *34*, 811–813.
- (24) Fukuyama, Y.; Iwamoto, S.; Tanaka, K. *J. Mass Spectrom.* **2006**, *41*, 191–201.
- (25) Quinton, L.; Demeure, K.; Dobson, R.; Gilles, N.; Gabelica, V.; De Pauw, E. *J. Proteome Res.* **2007**, *6*, 3216–3223.
- (26) Nicolardi, S.; Switzer, L.; Deelder, A. M.; Palmblad, M.; van der Burgt, Y. E. *Anal. Chem.* **2015**, *87*, 3429–3437.
- (27) Marshall, A. G.; Verdun, F. R. *Fourier Transforms in NMR, Optical, and Mass Spectrometry*; Elsevier, 1990, ISBN 9781483293844.
- (28) Xian, F.; Hendrickson, C. L.; Blakney, G. T.; Beu, S. C.; Marshall, A. G. *Anal. Chem.* **2010**, *82*, 8807–8812.
- (29) Qi, Y.; Thompson, C. J.; Van Orden, S. L.; O'Connor, P. B. *J. Am. Soc. Mass Spectrom.* **2011**, *22*, 138–147.
- (30) Lange, O.; Damoc, E.; Wieghaus, A.; Makarov, A. *Int. J. Mass Spectrom.* **2014**, *369*, 16–22.
- (31) Kilgour, D. P. A.; Wills, R.; Qi, Y.; O'Connor, P. B. *Anal. Chem.* **2013**, *85*, 3903–3911.
- (32) Srzentic, K.; Fornelli, L.; Tsybin, Y.; Loo, J.; Agar, J.; Chamot-Rooke, J.; Danis, P.; Ge, Y.; Goodlett, D.; Kelleher, N.; Pasa Tolic, L.; Smith, L.; Toby, T.; Nagornov, K.; Brodbelt, J.; Greer, S.; Dupré, M.; Clarke, D.; Lin, Z.; Haselmann, K., et al. *66th ASMS Conference on Mass Spectrometry and Allied Topics 2018*; San Diego, CA, 2018; Poster ID 294106.
- (33) Sjögren, J.; Olsson, F.; Beck, A. *Analyst* **2016**, *141*, 3114–3125.
- (34) Vincents, B.; Guentsch, A.; Kostolowska, D.; von Pawel-Rammigen, U.; Eick, S.; Potempa, J.; Abrahamson, M. *FASEB J.* **2011**, *25*, 3741–3750.
- (35) Kilgour, D. P. A.; Neal, M. J.; Soulby, A. J.; O'Connor, P. B. *Rapid Commun. Mass Spectrom.* **2013**, *27*, 1977–1982.
- (36) Kilgour, D. P. A.; Nagornov, K. O.; Kozhinov, A. N.; Zhurov, K. O.; Tsybin, Y. O. *Rapid Commun. Mass Spectrom.* **2015**, *29*, 1087–1093.
- (37) Kilgour, D. P. A.; Van Orden, S. L. *Rapid Commun. Mass Spectrom.* **2015**, *29*, 1009–1018.
- (38) Kilgour, D. P. A.; Van Orden, S. L.; Tran, B. Q.; Goo, Y. A.; Goodlett, D. R. *Anal. Chem.* **2015**, *87*, 5797–5801.
- (39) Strohal, M.; Hassman, M.; Košata, B.; Kodíček, M. *Rapid Commun. Mass Spectrom.* **2008**, *22*, 905–908.
- (40) Loos, M.; Gerber, C.; Corona, F.; Hollender, J.; Singer, H. *Anal. Chem.* **2015**, *87*, 5738–5744.
- (41) Smith, D. F.; Podgorski, D. C.; Rodgers, R. P.; Blakney, G. T.; Hendrickson, C. L. *Anal. Chem.* **2018**, *90*, 2041.
- (42) Anderson, L. C.; DeHart, C. J.; Kaiser, N. K.; Fellers, R. T.; Smith, D. F.; Greer, J. B.; LeDuc, R. D.; Blakney, G. T.; Thomas, P. M.; Kelleher, N. L.; Hendrickson, C. L. *J. Proteome Res.* **2017**, *16*, 1087–1096.
- (43) Nicolardi, S.; van der Burgt, Y. E. M.; Codée, J. D. C.; Wuhrer, M.; Hokke, C. H.; Chiodo, F. *ACS Nano* **2017**, *11*, 8257–8264.
- (44) Srzentic, K.; Nagornov, K. O.; Fornelli, L.; Lobas, A. A.; Ayoub, D.; Kozhinov, A. N.; Gasilova, N.; Menin, L.; Beck, A.; Gorshkov, M. V.; Aizikov, K.; Tsybin, Y. O. *Anal. Chem.* **2018**, *90*, 12527–12535.
- (45) Fornelli, L.; Ayoub, D.; Aizikov, K.; Liu, X.; Damoc, E.; Pevzner, P. A.; Makarov, A.; Beck, A.; Tsybin, Y. O. *J. Proteomics* **2017**, *159*, 67–76.
- (46) Cotham, V. C.; Brodbelt, J. S. *Anal. Chem.* **2016**, *88*, 4004–4013.
- (47) Fornelli, L.; Srzentić, K.; Huguet, R.; Mullen, C.; Sharma, S.; Zabrouskov, V.; Fellers, R. T.; Durbin, K. R.; Compton, P. D.; Kelleher, N. L. *Anal. Chem.* **2018**, *90*, 8421–8429.
- (48) De Leoz, M. L. A.; Duewer, D. L.; Stein, S. E. *NIST Interlaboratory Study on the Glycosylation of NISTmAb*; NIST Report 8186; National Institute of Standards and Technology, U.S. Department of Commerce, 2017; DOI: 10.6028/NIST.IR.8186.
- (49) Hilliard, M.; Alley, W. R., Jr.; McManus, C. A.; Yu, Y. Q.; Hallinan, S.; Gebler, J.; Rudd, P. M. *mAbs* **2017**, *9*, 1349–1359.
- (50) Nicolardi, S.; Deelder, A. M.; Palmblad, M.; van der Burgt, Y. E. M. *Anal. Chem.* **2014**, *86*, 5376–5382.